J. Fluid Mech. (1997), *vol.* 339, *pp.* 391–411

Thermally driven motions in a rotating stratified fluid: theory and experiment

By J. PEDLOSKY[1], J. A. WHITEHEAD[1] AND GRAHAM VEITCH[2]

[1] Physical Oceanography Department, Woods Hole Oceanographic Institution, Woods Hole, MA 02543, USA

[2] Department of Applied Mathematics and Theoretical Physics, University of Cambridge, Silver Street, Cambridge CB3 9EW, UK

(Received 12 September 1996 and in revised form 20 December 1996)

A radial temperature distribution is applied to the top of a cylinder of rotating stably stratified fluid. Thermal wind shear drives the interior flow. Linearized theory predicts, and laboratory experiments confirm, that when the stratification is large enough it completely suppresses the Ekman pumping into the interior. The interior velocity field, which is primarily azimuthal, responds by satisfying the no-slip boundary conditions without the need of Ekman layers on the horizontal surfaces. Moreover, for large stratification a thermal boundary layer beneath the top surface traps the thermal disturbance applied at the upper surface. The greatest azimuthal velocity occurs at the base of this layer. Below this layer the azimuthal velocity viscously diffuses downward with thermal wind adjusting the temperature. The Rossby radius of deformation based on this layer depth is the cylinder's radius divided by the square root of the Prandtl number. Detailed measurements of the velocity field generated in the cylinder by the heating are compared with the theory in the case where the Ekman layers are eliminated by stratification. The theory and experiments agree qualitatively well over a range of four orders of magnitude of imposed parameters and over a large parameter range the quantitative comparison is also very good.

1. Introduction

The present study arose as a consequence of an attempt to understand the circulation of the Black Sea and similar small ocean basins. A series of studies (Bulgakov 1987; Bulgakov, Korotaev & Whitehead 1996*a*, *b*, 1997) has attempted to describe and deal especially with the phenomenon of buoyancy forcing of the circulation of the Black Sea. Although it is generally believed that the overall cyclonic circulation of the Black Sea has a strong wind-driven component, the role of buoyancy forcing as an important component of the forcing is suggested in the papers referenced above. In particular, the role of river run-off and its associated salinity anomalies provide a plausible mechanism for buoyancy forcing of the circulation. Interchange of water with the sea of Marmara through the Bosphorous Straits represents another possible source of buoyancy forcing. Several visits to the Woods Hole Oceanographic Institution in the last decade by Ukrainian oceanographers led to a series of laboratory experiments carried out there in which fresh water and salinity forcing was simulated by the introduction of fresh and saline water at various locations along the rim of a rotating cylinder of water. Other laboratory attempts to model such buoyancy forcing involved thermally driving the flow by heating the cylindrical container along its sides. For

example, in one case a high temperature was imposed on the upper surface of the cylinder while the outer rim was cooled. Or, in another, the heating and cooling were introduced on the sidewall by exposing the upper half of the cylinder to a temperature bath at higher temperature than the lower half. In all cases a strongly baroclinic circulation was observed in rough qualitative agreement with the predictions of a very simple physical theory. The underlying theory assumed the internal density field in the fluid was established entirely by diffusion and the azimuthal velocity in the basin then was calculated by thermal wind considerations, i.e. by the application of the geostrophic and hydrostatic approximations. Quantitative agreement between the experiments and theory was poor. This was probably due to the absence of advective effects of density in the theory and also to the rather difficult theoretical problem posed by the experiments in which the static stability of the fluid is eliminated at the position of the forcing whenever the temperature on the rim is made locally independent of depth.

An attempt was therefore made to construct an experiment which would allow a more careful comparison between the experimental results and theory. To that end we set up a configuration in which a rotating cylinder of fluid was endowed with a nearly uniform vertical stratification with, in addition, a very small radial temperature variation imposed on the upper surface. This surface temperature forcing was axially symmetric and was of small enough amplitude so that the fluid was always stably stratified. The experimental apparatus is described in more detail in §2.

It is clear that the resulting physical system is now quite far from being a realistic model of the circulation of the Black Sea or perhaps any real oceanographic flow. We tend to view it, as described above, as a way-station in our attempt to find a situation in which careful laboratory measurements can be compared to theory as a starting point for more difficult and realistic experiments in the future. The simplicity of the present experiment allows the effects of advection of density to be dealt with within the context of a linearization of the temperature equation as described in §3 below.

The theory that is used in this study is a minor extension of the theory developed nearly three decades ago and described in a series of papers by Barcilon & Pedlosky (1967*a–c*). See also Veronis (1967). The theory of Barcilon & Pedlosky is a linear theory in which the advection of momentum is ignored and the advection of density is modelled by the vertical advection of a large vertically varying $O(1)$ stratification. There have been few opportunities for a detailed comparison of the results of that theory with laboratory experiments and so another motive of the present study is to examine how well this linearized theory, described in detail in §3, can reproduce and explain the principal experimental results.

The comparison between theory and experiment is described in §4. Rather astonishingly, given the idealizations of the linear theory, we find satisfying quantitative agreement between the theory and experiments. In particular, the theory predicts, in the limit of large stratification, the existence of internal jets whose maximum velocities occur at a depth which depends on stratification so that, as the stratification strengthens, the velocity maximum becomes closer to the upper surface of the fluid where it is heated. The depth of maximum velocity is such that a Rossby deformation radius based on that depth is equal to the cylinder radius divided by the square root of the Prandtl number.

Another prediction of the theory is the quenching of the Ekman layer suction on the horizontal rigid surfaces of the cylinder when the stratification exceeds a critical level. Although these boundary layers are a controlling influence for weakly stratified fluids (Greenspan 1968) through the mechanism of Ekman suction and pumping, strongly

stratified flows can eliminate the need for the Ekman layers by allowing the inviscid interior flow to satisfy the no-slip boundary condition directly. This is described more completely in §3 but a principal result of the present study is the demonstration of this phenomenon in the experiment.

The last section of the paper, §5, reviews the principal results of our study and describes plans for future experiments in which the comparison with theory is a key feature of the experimental configuration.

2. The experiment

In order to allow a careful comparison between theory and experiment it was desired to produce uniformly rotating fluid which could then be stratified and placed into motion by imposing a radially variable temperature on the upper surface. The device which was used to achieve this result consisted of a rotating container with two coaxial Plexiglas cylinders on an aluminium base with a medal lid as shown in figure 1. The bottom temperature was maintained by flushing the 1 cm thick aluminium plate continuously with cold water from a refrigerated bath at a temperature T_b. The top temperature distribution was imposed by using a circular stainless steel lid 3 mm thick and 22 cm in radius which was heated as follows.

In a region of radius 2.75 cm near the middle of the upper plate, a cylindrical tube was bolted to the lid and contained water fed from a thermostatic bath at temperature T_i. Near the outer circumference at 22 cm from the centre, there was a circular loop of copper tubing silver-soldered to the lid. It was fed by water from a second hot bath at temperature T_o. Thermal conduction through the metal plate was intended to establish a smooth and monotonic conductive transition between the temperatures of the two baths at T_i and T_o. In practice, the downward conduction of heat into the fluid was non-negligible and the surface distribution of temperature, which represents the forcing of the motion in the container, was non-monotonic with a temperature minimum about halfway between the inner and outer radii of the cylinder. To determine the actual radial distribution of temperature which is used as a boundary condition for the theory, the apparatus' lid was fitted with five thermocouples glued in holes at radii of 0, 4, 8, 12 and 16 cm from the centre. In some of the later experiments the temperature was measured at 2 cm intervals from the centre but the measurements gave a temperature distribution which differed negligibly from the previous distributions from the five thermocouples.

The outer wall of the cylindrical tank had an inside diameter of 44.5 cm but to reduce heat loss and mimic insulation of the outer vertical boundary a second wall with an inside diameter of 33 cm was inserted. The test section was within this inner wall; the outer annular chamber presumably contained a stratified fluid which matched the vertical stratification of the test chamber. The top lid rested directly on this false sidewall to make a test chamber 9.8 cm deep. The outer cylinder of the tank and the top lid were closely encased with 5 cm of rubber foam for thermal insulation so that heat loss to the air was reduced as much as possible with respect to the heat flux into the fluid from the plates. The top lid was unfortunately slightly distorted by soldering during construction so that it was warped by about 2 mm from being truly flat. The warp was axially symmetric and was most pronounced at radii beyond 16 cm and thus is small in the test section. There may be some small quantitative effect of the warp on the flow by altering very slightly the actual applied radial temperature gradient. We believe the effect is qualitatively negligible.

The tank and the three baths were mounted on a 1 m diameter rotating turntable

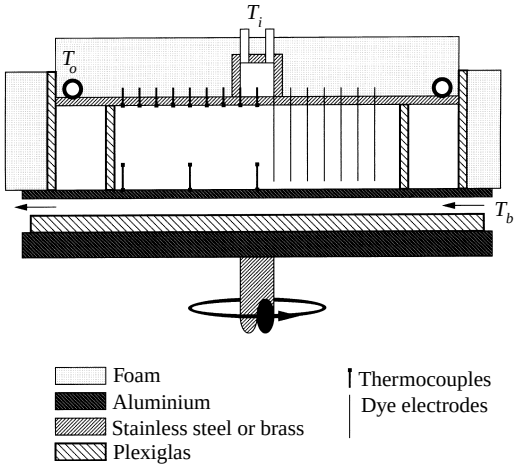

FIGURE 1. A schematic view of the experimental apparatus. The working fluid is contained in the open region within the inner boundary indicated in the figure while the fluid is heated at the upper surface and cooled at the lower surface as described in the text.

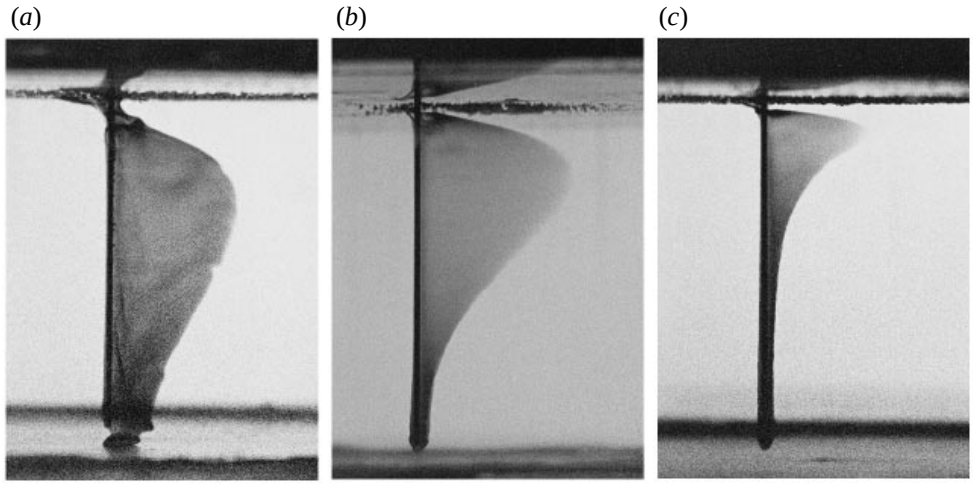

FIGURE 2. The dye streaks demonstrating the profile of azimuthal velocity in the experiment: (*a*) $S = 0.014$, (*b*) $S = 0.15$, (*c*) $S = 29$.

with a rotation rate adjustable to 0.001 s^{-1}. Runs were conducted by setting thermostat values and commencing rotation. Care was taken to ensure that the fluid had arrived at a steady state before taking data. Temperatures of 15 thermocouples were monitored every 600 s and automatically stored so that the evolution of the temperature field could be reproduced. These 15 thermocouples were located at the five radii in the upper lid as described previously; four were 0.9 cm below the top lid at radii of 2, 6, 10 and 14 cm from the centre while three were located at 4 cm above the bottom at 0, 8 and 16 cm from the centre. Finally another three thermocouples were located on the bottom directly below the three that were placed at 4 cm above the bottom. It was clear from monitoring these thermocouples that it took about 6 hours for the temperature field in the experiments to achieve a steady state.

The flow was visualized with a thymol blue technique. Thymol blue solution, a pH sensitive indicator, was buffered to the yellow side of its transition pH. Vertical brass rod electrodes were spaced at 2 cm radial intervals from 2 to 14 cm. When 1.5 V was applied, the solute around the negative electrode changed to a dark blue with little change of fluid density. The fluid flow was predominantly azimuthal as a consequence of the axial symmetry of the forcing and this velocity was indicated by the motion of the dye away from the wire. This technique is particularly well suited for measuring slow flows. In the present case the observed fluid velocities were less than 0.06 cm s^{-1} and this method worked quite well although in a few cases buoyant effects were noted in the dye after a few minutes.

The principal measured quantity was the azimuthal velocity. During a velocity measurement the side insulation was removed and the tank was backlit with fluorescent lights. Images of the dye were recorded continuously on video tape as the tank spun in front of the camera. As time progressed, die streaks were swept away from the electrode and a profile could be measured later by freezing video frames and measuring dye displacement. Lengths on the screen were calibrated by measurements of the profile of a 1.27 cm ball that was placed at different radii to correct for magnification produced by the curved cylindrical walls. Successive measurements divided by the time interval gave the velocity. Photographic examples of such dye streaks are shown in figure 2.

For the range of parameters of these experiments the appropriate measure of stratification is

$$S = \alpha g \Delta T_v / (f^2 L), \tag{2.1}$$

where α is the coefficient of thermal expansion, g is the acceleration due to gravity, ΔT_v is the temperature difference between the upper and lower plates of the cylinder, f is twice the rotation rate of the cylinder and L is the cylinder's depth. This can also be expressed simply as $S = N^2/f^2$ where N is the Brunt–Väisälä frequency of the stratified fluid.

In figure 2(*a*) the velocity profile is shown for a case of small stratification, $S = 0.014$ while figure 2(*b*) shows the profile for a moderate value, $S = 0.15$. Figure 2(*c*) shows the profile of azimuthal velocity for the fairly large $S = 29$. Note how the maximum of the profile retreats to the upper boundary as the stratification increases. This is one of the principal qualitative predictions of the theory. Note also the manner in which the velocity smoothly goes nearly to zero at the upper and lower boundaries without the need for Ekman layers to satisfy the no-slip conditions. A weak Ekman layer can be still seen in the photos, manifested by the small gaps between the profile and each boundary where the Ekman layers are transporting fluid radially.

The velocity profiles at 2 cm intervals from 2 to 14 cm from the centre were measured and digitized. A typical set of profiles is shown in figure 3. The velocity is zero at the upper boundary with increasing magnitude with depth. Each profile reaches a maximum somewhere in the upper half of the tank and then decreases smoothly with depth and very nearly vanishes at the cylinder's bottom. The velocity profiles are generally prograde at small radius and retrograde at large radius, reflecting the minimum in the surface temperature forcing at mid-radius that was mentioned above. It is particularly important to note that although the forcing is purely thermal rather than mechanical, the velocity profiles at each radius are very nearly of a single sign. There are no substantial reversals of the velocity with depth as one might expect for a strongly baroclinic flow. In §3 this is shown to be related to the suppression of the Ekman pumping by the stratification.

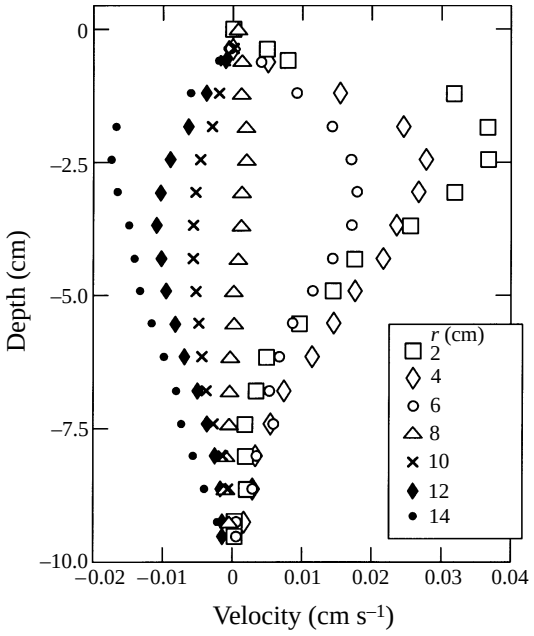

FIGURE 3. Velocity profiles from the 12/1 experiment in which S is 0.15.

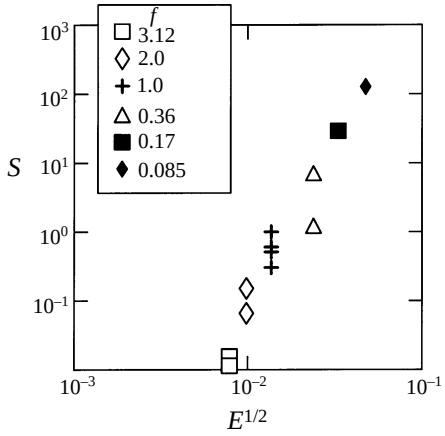

FIGURE 4. A summary of the parameter space of the experiments.

Experimental runs were conducted over as wide a range of parameters as possible. The appropriate measure of viscosity in the experiment is the Ekman number,

$$E = 2\nu/(fL^2) \tag{2.2}$$

where ν is the coefficent of kinematic viscosity. Figure 4 shows a summary of the parameters of the experiments in the $(S, E^{1/2})$-plane. A more detailed list of the experiments, with the relevant experimental parameters, is given in table 1. The experiments are coded by date. Note that $S \gg E^{1/2}$ in most of the cases which, as we see below, has important physical consequences; in particular, the theory predicts the elimination of the Ekman layers in this limit. The Rossby number, ϵ, is defined below

Date	S	$E^{1/2}$	ϵ	f (s^{-1})	ΔT_v (°C)	$L/(\sigma S)^{1/2}$ (cm)
5/17	116	0.048	29	0.085	30	0.38
5/16	29	0.033	6.15	0.17	30	0.79
5/10	8.68	0.024	2.31	0.36	30	1.6
5/14	1.08	0.023	0.60	0.36	5	3.9
1/22	0.85	0.014	0.26	1.0	30	4.5
5/3	0.56	0.014	0.15	1.0	20	5.7
1/9	0.52	0.014	0.16	1.0	20	5.9
12/7	0.3	0.014	0.11	1.0	10	7.8
12/1	0.15	0.010	0.04	2.0	20	11
1/10	0.07	0.010	0.02	2.0	10	16
1/25	0.014	0.008	0.008	3.12	5	36
1/24	0.012	0.008	0.003	3.12	4	39

TABLE 1. List of experiments and their parameters

(equation (3.5)) while σ is the Prandtl number, i.e. the ratio of kinematic viscosity to thermal diffusivity. The vertical temperature difference between the upper and lower boundary of the cylinder is ΔT_v.

Direct observations of the flow showed that it is eventually steady and axially symmetric for all of the cases studied. There is no hint of instability of either the classical baroclinic type or of symmetric instability. The former is probably eliminated by the large values of the stratification (Pedlosky 1987) while the latter is similarly unlikely due to the combination of small Rossby number (defined below) and high stratification of the flow so that the flow is in the stable regime for symmetric instability (McIntyre 1970). These experimental facts allow the construction of a fairly simple laminar theory for the experiment which is taken up in the following section.

3. Theory

Based on the experimental results, we develop a theory for axially symmetric motion in a cylinder of depth L and radius r^*. The cylinder is spinning with angular velocity $\Omega = f/2$ and the fluid is considered to be incompressible and satisfies the Boussinesq approximation. The temperature in the cylinder is partitioned as follows:

$$T_{\mathrm{dim}} = T_{oo} + \Delta T_v (z/L) + \Delta T_h \, T(r, z). \tag{3.1}$$

The temperature scale ΔT_v is the vertical temperature change which occurs linearly from top to bottom in deviation from T_{oo}. It is a solution to the thermal conduction equation in the absence of motion (and ignoring the small centrifugal effects due to rotation). The second scale, ΔT_h, is the characteristic amplitude of the temperature perturbation due to the heating of the upper surface as described in §2. A linear equation of state relating temperature and density is used. The fundamental assumption of the theory is that

$$\Delta T_h / \Delta T_v \ll 1. \tag{3.2}$$

The independent and dependent variables are scaled as follows. Both the vertical and horizontal lengths are scaled with L. The temperature anomaly is scaled, as in (3.1), with ΔT_h. The characteristic scale, U, for the horizontal velocity is determined from an anticipation of geostrophic and hydrostatic balance for the azimuthal velocity so that

$$U = \alpha g \, \Delta T_h / f. \tag{3.3}$$

The pressure scale is $P = \rho_o UfL$. In terms of these scales the non-dimensional equations of motion are

$$\epsilon\{uu_r + wu_z - v^2/r\} - v = -p_r + \tfrac{1}{2}E[\nabla^2 u - u/r^2], \tag{3.4a}$$

$$\epsilon\{uv_r + wv_z + uv/r\} + u = \tfrac{1}{2}E[\nabla^2 v - v/r^2], \tag{3.4b}$$

$$\epsilon\{uw_r + ww_z\} = -p_z + T + \tfrac{1}{2}E[\nabla^2 w], \tag{3.4c}$$

$$\frac{1}{r}(ru)_r + w_z = 0, \quad \epsilon\{uT_r + wT_z\} + wS = \frac{E}{2\sigma}\nabla^2 T, \tag{3.4d, e}$$

where

$$\nabla^2 = \frac{1}{r}\left(\frac{\partial}{\partial r} r \frac{\partial}{\partial r}\right) + \frac{\partial^2}{\partial z^2};$$

otherwise, subscripts denote differentiation.

The radial velocity is u, the azimuthal velocity is v and the vertical velocity is w. The Prandtl number $\sigma = \nu/\kappa$, i.e. the ratio of the kinematic viscosity to the thermal diffusivity.

The Rossby number is defined as

$$\epsilon = \frac{U}{fL} = \frac{\Delta T_h}{\Delta T_v} S. \tag{3.5}$$

Note that even this relatively simple problem has four dimensionless parameters: ϵ, E, S and σ.

Since the motion is axially symmetric the azimuthal pressure gradient is zero and so the geostrophic radial velocity is zero. The non-dimensional temperature is $O(1)$ as is the pressure and azimuthal horizontal velocity. This leads to a presumptive estimate for the non-dimensional radial velocity, $u = O(E)$. Further analysis shows that $w \leqslant O(E^{1/2})$ and, in fact, over the parameter range of interest for which σS is $O(1)$ it can be shown that w is $O(E)$ itself. Thus as long as $\epsilon \ll 1$ the nonlinear advection of momentum can be ignored in (3.4*a–c*). A similar analysis shows that as long as $\epsilon/S \ll 1$ the nonlinear advection can be ignored in the thermal equation (3.4*e*). When these conditions are fulfilled this yields the reduced linear set:

$$-v = -p_r + \tfrac{1}{2}E[\nabla^2 u - u/r^2], \quad u = \tfrac{1}{2}E[\nabla^2 v - v/r^2], \tag{3.6a, b}$$

$$0 = -p_z + T + \tfrac{1}{2}E[\nabla^2 w], \quad \frac{1}{r}(ru)_r + w_z = 0, \quad wS = \frac{E}{2\sigma}\nabla^2 T. \tag{3.6c–e}$$

Ekman layers may exist on the upper and lower surfaces of the cylinder. Standard boundary layer analysis provides a compatibility condition that the bulk of the flow must satisfy (Pedlosky 1987)

$$w = (-1)^z \frac{E^{1/2}}{2}\frac{1}{r}[rv(r,z)]_r, \quad z = (0,1), \tag{3.7}$$

where $v(r,z)$ is the fluid velocity just outside the Ekman layers.

The boundary conditions for T on these boundaries are

$$\left.\begin{aligned} T &= 0, & z &= 0, \\ T &= T_u(r), & z &= 1, \end{aligned}\right\} \tag{3.8}$$

where $T_u(r)$ is the known temperature applied at the upper surface. The outer radius

of the cylinder in non-dimensional units is $r_o = r^*/L$. On $r = r_o$, the outer rim of the cylinder, the velocity is zero and the radial temperature gradient vanishes since the wall of the cylinder is insulated.

The temperature in the cylinder can be anticipated to be $O(1)$ from (3.8). This implies from (3.6*e*) an estimate for the vertical velocity in the interior of the fluid of $O(E/\sigma S)$. Yet (3.7) suggests that the Ekman layers will normally pump a vertical velocity of $O(E^{1/2})$ into the interior. If $\sigma S \gg E^{1/2}$, which is the parameter domain of the experiment, the Ekman layers will pump a velocity larger than the interior can absorb. Barcilon & Pedlosky (1967*b*) show that this paradox is resolved by having the interior flow adjust its azimuthal velocity so that, to lowest order, the interior v vanishes on the upper and lower boundaries of the cylinder.

Before proceeding we demonstrate the vanishing of the interior azimuthal velocity at the upper and lower boundaries by examining the interior flow in the parameter range $\sigma S \ll 1$. This is generally not the range of the parameters for the experiment but it is a very illuminating parameter setting to examine the transformation of the behaviour of the flow which is relevant to the experimental conditions.

For small σS there are two boundary layers on the sidewall of the cylinder. The thinner one has a non-dimensional thickness

$$\delta_b = \frac{1}{L}\left(\frac{4\nu\kappa L}{\alpha g\,\Delta T_v}\right)^{1/4} = \frac{E^{1/2}}{(\sigma S)^{1/4}} \tag{3.9}$$

and is called the buoyancy layer by Barcilon & Pedlosky. Its dynamics are non-hydrostatic and its function in the present circumstance is only to help satisfy the no-slip condition on the weak vertical velocity. It will not be considered further.

A wider boundary layer exists whose non-dimensional thickness is

$$\delta_h = [\sigma S]^{1/2}, \tag{3.10}$$

which normally serves to close the circulation in the vertical plane. However, with insulating conditions on the sidewall it is possible to show that the boundary layer is inactive to lowest order. In that case the problem reduces to the problem for the interior in which, for $\sigma S \ll 1$ it follows from (3.6*b*) that u is $O(E)$ while w is larger and is $O(E/\sigma S)$. Hence from (3.6*d*) it follows that to $O(\sigma S)$

$$w_z = 0 \tag{3.11}$$

in the interior. Thus, if ψ is the streamfunction for the velocity in the (r, z)-plane, i.e. if

$$w = \frac{1}{r}\psi_r, \quad u = -\frac{1}{r}\psi_z, \tag{3.12a, b}$$

it follows that in this limit ($\sigma S \ll 1$) ψ is a function only of r. Barcilon & Pedlosky (1967*c*) show that using the Ekman compatibility conditions, (3.7), the thermal wind relation for v,

$$v_z = T_r \tag{3.13}$$

allows ψ to be written as

$$\psi = -\tfrac{1}{4}E^{1/2} r \int_0^1 T_r \,\mathrm{d}z \tag{3.14a}$$

and

$$v = \int_0^z T_r \,\mathrm{d}z' - \frac{1}{2}\int_0^1 T_r \,\mathrm{d}z. \tag{3.14b}$$

Note that ψ is identically zero on the rim of the cylinder where the radial temperature gradient vanishes. From the thermal wind this also implies that v vanishes there as well. This demonstrates the ability of the interior fields to satisfy all but the no-slip condition on w at $r = r_o$.

A key parameter of the problem is the ratio

$$\lambda = \frac{\sigma S}{2E^{1/2}}. \tag{3.15}$$

Although σS has been assumed to be small, the size of the parameter λ is arbitrary. When λ is small the fluid acts as an unstratified fluid in the sense that the Ekman pumping dominates the dynamics. When λ is large the stratification suppresses the interior vertical velocity to a level below that which an order 1 azimuthal velocity at the horizontal surfaces will pump into the interior. If (3.12a) and (3.14a) are used in (3.6e) it can be shown that the temperature satisfies,

$$\nabla^2 \Theta = 0, \tag{3.16}$$

where

$$\Theta = T(r,z) + \lambda \int_0^1 T(r,z)\,\mathrm{d}z. \tag{3.17}$$

Note that

$$w = -\tfrac{1}{4}E^{1/2}\frac{1}{r}\frac{\partial}{\partial r}r\frac{\partial}{\partial r}\int_0^1 T\,\mathrm{d}z. \tag{3.18a}$$

The equivalent temperature Θ satisfies the conduction equation but includes the effects of linearized advection through (3.14). In terms of Θ

$$T = \Theta - \frac{\lambda}{1+\lambda}\int_0^1 \Theta\,\mathrm{d}z. \tag{3.18b}$$

On the outer wall of the cylinder both Θ and T satisfy the zero radial derivative condition. The solution is completed by applying the conditions (3.8) on T in (3.18b). In the limit of large λ the temperature T will have from (3.18b) a vertical average which will be of order (λ^{-1}). Thus, from (3.18a) w will be of the order of $E/\sigma S$ for $\lambda \gg 1$, i.e. much less than that estimated from the Ekman pumping condition.

To examine the character of the solution we consider first a simple illustrative example in which the upper temperature is a monotonically increasing function of r, namely

$$T_u = \mathrm{e}^{r/r_o} - 1.$$

Figure 5 shows the azimuthal velocity at the mid-radius of the cylinder, $r = 0.5r_o$, for three values of λ. In figure 5(a) the azimuthal velocity is shown for the small value of $\lambda = 0.01$ for which the fluid acts as if it were unstratified. In this limit the vertical advection in the mean temperature gradient is inconsequential and the temperature field is established by pure conduction. Indeed, in this limit there is little difference between T and Θ. The azimuthal velocity is cyclonic near the upper surface and the Ekman velocity pumped downward passes unaltered to the lower surface where it is absorbed in the lower Ekman layer. Note that v is equal but of opposite sign at the two boundaries as it must be from (3.7). The asymmetry in the v-profile, i.e. the fact that the zero of v occurs for $z \approx 0.81$, is due to the larger vertical shear in the upper region of the fluid where the heating takes place. The thermal wind vanishes at the lower surface where the radial temperature gradient is zero in response to the boundary

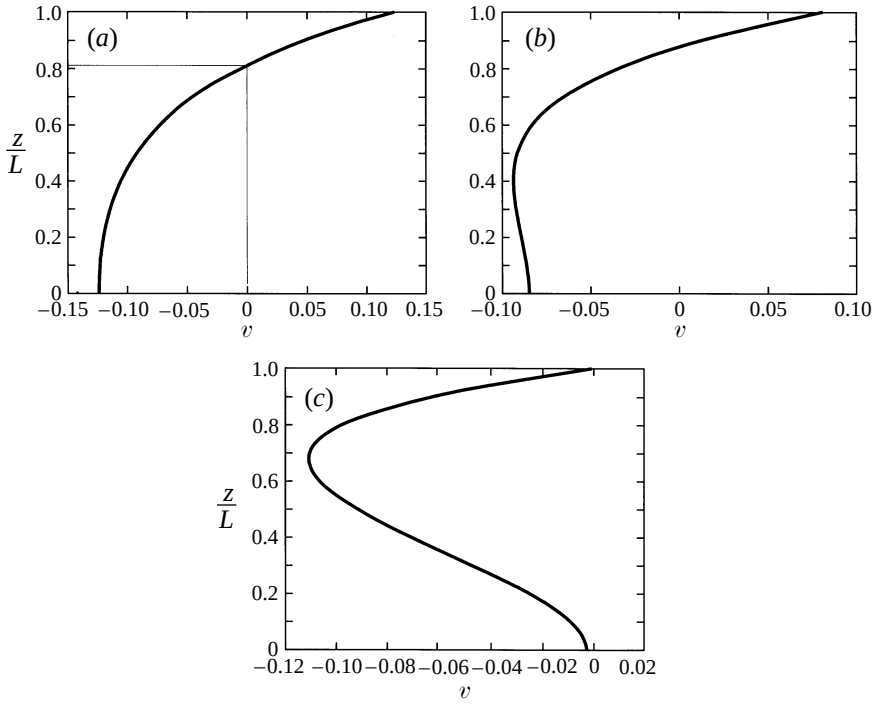

FIGURE 5. The azimuthal velocity profile in the example in which the temperature distribution on the upper plate is $T_u = e^{r/r_o} - 1$. The profile is shown at $r = 0.5r_o$. (*a*) $\lambda = 0.01$, (*b*) $\lambda = 1.0$, (*c*) $\lambda = 100$.

condition. In this limit the flow is baroclinic but the control of the fluid by the Ekman layers still reflects a strong barotropic dynamics.

In 5(*b*), $\lambda = 1$. Note that the azimuthal velocity is smaller in magnitude at the upper and lower surfaces than in the previous example. This is an indication of the quenching effect of the stratification on the Ekman pumping. As the stratification increases the magnitude of the vertical velocity must decrease. For $\sigma S \gg E^{1/2}$ the vertical velocity is $O(E/\sigma S)$ and is less than $E^{1/2}$, in which case v must go to zero on the lateral boundaries of the cylinder. This is shown in figure 5(*c*) in which the case $\lambda = 100$ is shown. In this limit the azimuthal velocity of the interior flow very nearly satisfies the no-slip boundary condition at $z = 0$ and $z = 1$. The azimuthal velocity is now an entirely retrograde jet with a maximum above the mid-point of the depth. The thermal wind shear is positive near $z = 1$ as specified by the surface temperature condition. That, coupled with the condition that v must be zero there in order to quench the Ekman pumping, forces v to become increasingly negative in the region below the upper lid of the cylinder. The v-profile must return to nearly zero at $z = 0$. Since the temperature is horizontally uniform at the lower boundary the vertical shear of v due to the thermal wind balance should be zero at $z = 0$. The slight departure of the thermal wind shear in the figure from zero at the lower boundary reflects only a minor inadequacy in plotting routine.

Thus as long as $\sigma S \gg E^{1/2}$ the Ekman layers are an inconsequential factor in the dynamics.

In the interior the azimuthal velocity is always in geostrophic and hydrostatic balance. This allows a single equation for the pressure to govern the motion in the range $E^{1/2} \ll \sigma S \ll E^{-1}$.

A straightforward manipulation of the momentum equations allows us to obtain

$$[1+\tfrac{1}{4}E^2\nabla^4](\boldsymbol{\nabla}_h\cdot\boldsymbol{u}) = \tfrac{1}{2}E\nabla^2\nabla_h^2 p, \tag{3.19}$$

where

$$\nabla_h^2 = \frac{1}{r}\frac{\partial}{\partial r}r\frac{\partial}{\partial r}$$

and $\boldsymbol{\nabla}_h\cdot\boldsymbol{u}$ is the divergence of the horizontal velocity.

For motions with length scales greater than that of the Ekman layer ($E^{1/2}$), the second term in the square bracket on the left-hand side of (3.19) is negligible. Using the continuity equation, the hydrostatic approximation and the thermal equation, (3.6*e*), we can obtain a single equation for the pressure which holds in the interior, outside the Ekman layers, which as we have seen are relatively inconsequential features in this parameter regime.

Thus the pressure satisfies:

$$\nabla^2\left[\sigma S\nabla_h^2+\frac{\partial^2}{\partial z^2}\right]p = 0. \tag{3.20}$$

The vorticity balance leading to (3.20) is simply

$$0 = \frac{\partial w}{\partial z}+\tfrac{1}{2}E\nabla^2\zeta, \tag{3.21),}$$

where ζ is the vertical component of the relative vorticity. When (3.21) is combined with the thermal equation and the geostrophic approximation is used to express ζ in terms of the pressure, (3.20) follows directly.

It is easily seen that for small σS a boundary layer of width $(\sigma S)^{1/2}$ will occur on the outer wall of the cylinder in order to retain the order of the differential equation. As σS approaches unity this layer grows and fills out and becomes part of the interior. As σS increases further so that $\sigma S \gg 1$ a boundary layer appears near the upper horizontal plane. It has a thickness $(\sigma S)^{-1/2}$. A similar boundary layer could occur near the lower boundary of the cylinder but it is not required.

In the limit of large σS detailed but straightforward boundary layer analysis, not presented here, shows that the thermal forcing is trapped in this upper boundary layer. The resulting equation is simply the square bracket of (3.20) set equal to zero. The radial temperature gradient is $O(1)$ in this boundary layer so that over this depth of length $(\sigma S)^{-1/2}$ the azimuthal velocity changes by this amount. Since v must vanish at $z = 1$ (recall that the Ekman layer has been expunged at lowest order by the suppression of the Ekman pumping by the stratification) this allows the azimuthal velocity to grow to only $O((\sigma S)^{-1/2})$ at the edge of the boundary layer. The thermal forcing does not penetrate beneath that boundary layer and so the temperature perturbation, T, is zero. This implies that w must vanish below the boundary layer and this implies that u does also. Hence the circulation in the vertical plane is limited to the upper thermal boundary layer. Beneath that layer (3.6*b*) applies with $u = 0$. In this region the azimuthal velocity satisfies a diffusion equation: more precisely, p satisfies Laplace's equation in the region below the thermal boundary layer. In this region the velocity generated in the thermal boundary layer diffuses downward smoothly and matches the zero-velocity condition at the lower boundary. This, physically, is the nature of the solution in the high-stratification limit. Note that in this limit the streamfunction for u and w velocities will be $O(E)$ and limited to the thermal boundary layer region. This secondary circulation is closed in a very weak upper Ekman layer

which serves only to close the weak mass flux generated in the interior. Over the whole parameter range given before (3.19) the appropriate boundary conditions for (3.20) are

$$p_r = 0, \quad z = 0, 1, \tag{3.22a}$$

$$p_z = 0, \quad z = 0, \tag{3.22b}$$

$$p_z = T_u(r)\, z = 1. \tag{3.22c, d}$$

On the sidewall of the cylinder the only boundary layer for $\sigma S \geqslant 1$ is the buoyancy layer described above and with insulating boundary conditions its effect on the flow is inconsequential. It follows that on the outer rim of the cylinder the condition of no slip for the azimuthal velocity is satisfied by requiring

$$p_r = 0, \quad r = r_o. \tag{3.23}$$

The hydrostatic relation implies that the thermal insulating condition is matched automatically by (3.23) as a vertical derivative of the condition illustrates. It is also possible to show (and the results presented below will verify this) that the solution of (3.20) subject to (3.22) will also automatically satisfy $\psi = 0$ on $r = r_o$.

Thus, solutions of (3.20) can be sought in the form

$$p = \sum_{n=1} P_n(z)\, J_o(k_n\, r/r_o), \tag{3.24}$$

where k_n is the nth zero of the first Bessel function so that (3.23) is satisfied. The function P_n can be written as

$$P_n = A_n\, \mathrm{e}^{-q_n(z-1)} + B_n\, \mathrm{e}^{-q_n z} + C_n\, \mathrm{e}^{-q_n d(z-1)} + D_n\, \mathrm{e}^{-q_n dz}, \tag{3.25}$$

where $q_n = k_n/r_o$ and $d = (\sigma S)^{1/2}$. The coefficients A_n, $\mathrm{B_n}$, $\mathrm{C_n}$ and D_n are easily obtained by matching to the boundary conditions on $z = 0$ and 1. The only input required from the experiment, aside from the governing parameters, is the temperature distribution on $z = 1$. In the next section we present the results of our calculations for the laboratory cases and present the comparison between the theory and measurements. Note that in (3.25) the last two terms represent the thermal boundary layers possible on $z = 0$ and $z = 1$ while the first two terms represent the region where the azimuthal velocity works its way downward to the lower boundary by viscous diffusion. It is not difficult to show that (3.6e) requires

$$\psi = \frac{E}{\sigma S}\left[r p_{rz} + \int_0^r r' p_{zzz}\, \mathrm{d}r' \right] \tag{3.26}$$

from which it follows that ψ will differ from zero only within a region of order $(\sigma S)^{-1}$ of the upper surface.

4. Comparison of theory and experiment

Each experimental run corresponds to a given vertical temperature difference and rotation rate as given in table 1. These determined the parameters E and S. The horizontal temperature distribution of the upper lid was measured. Its overall amplitude of variation determined the Rossby number ϵ while its distribution with radius determined the structure of the flow driven in the cylinder and calculated from the linear theory. Note that in some cases the Rossby number is greater than unity.

However, the crucial nonlinearity is undoubtedly the advection of temperature; as noted in §2 it is the ratio of the Rossby number and S which measures the nonlinearity and that is always small.

The distribution of the surface temperature was measured at a number of radii and then fitted to a polynomial to use in the theory. For example, figure 6 shows the temperature distribution for experiment 12/1. Note that the temperature distribution is non-monotonic. It decreases sharply from the centre, has a minimum at about halfway to the cylinder's outer wall and then increases. This results, we believe, from the imperfect conductivity of the upper plate so that the monotonic conductive distribution from T_i to T_o was not realized. No matter: we can take this more complicated distribution as the boundary condition for the theory, and there is actually an advantage in this. From the discussion of §2 we expect a negative thermal wind shear in the inner zone of the cylinder where the radial temperature gradient is negative, and the opposite sign in the outer region. We therefore expect a prograde jet in the inner domain of the cylinder and a retrograde jet in the outer zone since $\sigma S/E^{1/2}$ is large (85.23) and the Ekman layer suction must be quenched. The experimental profiles of figure 3 demonstrate this quite clearly. The reversal of the flow is seen to occur in the vicinity of the profile taken at $r = 8$ cm in agreement with the position of the reversal of the temperature gradient.

Figure 7 shows the calculated velocity field. Figure 7(*a*) shows v in cm s^{-1} contoured in the (r, z)-plane. Positive v contours are solid, negative v is indicated by dashed lines. The two jets observed in the experiment are clearly in evidence. Figure 7(*b*) shows v as a function of depth at the positions at which the azimuthal velocity in the experiment was measured so that these profiles should be compared with those of figure 3. The agreement is generally very good. The amplitudes of the maximum positive and negative velocities are in close agreement although the computed retrograde jet is somewhat faster than the experimental value. At $r = 8$, where the velocities are weak and change sign, there is a substantial quantitative disagreement but this is to be expected since the signal is small there. One important feature of the motion that is predicted by the theory is the depth of the core of the velocity maximum, and there is relatively good agreement between theory and experiment. For example, the $r = 2$ cm profile has its experimental maximum at about 2 cm below the surface which is only slightly lower than that predicted by the theory.

Figure 7(*c*) shows the streamlines of the weak $O(E)$ meridional circulation in the (r, z)-plane for the interior. The circulation closes in the very thin and weak upper Ekman layer which is not resolved in the theory. Such velocities are too small to measure but it is interesting to note the double cell of the circulation driven by the reversal of the temperature gradient. The temperature anomaly is lowest near the mid-radius and this is the region of diffluence of the circulation as fluid moves, in the interior, both inward and outward from this radius.

In figure 8 the velocity profiles at two locations $r = 2$ and $r = 14$ are compared directly with the experimental data which are indicated with + symbols. Figure 8(*a*) shows the innermost profile, i.e. the profile with the largest measured prograde velocity. It is clear that the agreement is excellent both for magnitude and structure. Figure 8(*b*) shows the comparison at $r = 14$ cm. The agreement is quite good although as remarked above the computed maximum is slightly greater than that observed although the depth of the peak is well predicted. In this experiment σS is order 1(≈ 0.825) and we note the mid-depth range of the meridional circulation. The thermal boundary layer is fat and the full equation (3.20) is required to obtain an accurate solution. It is important to emphasize that this solution, which ignores the frictional forces acting on

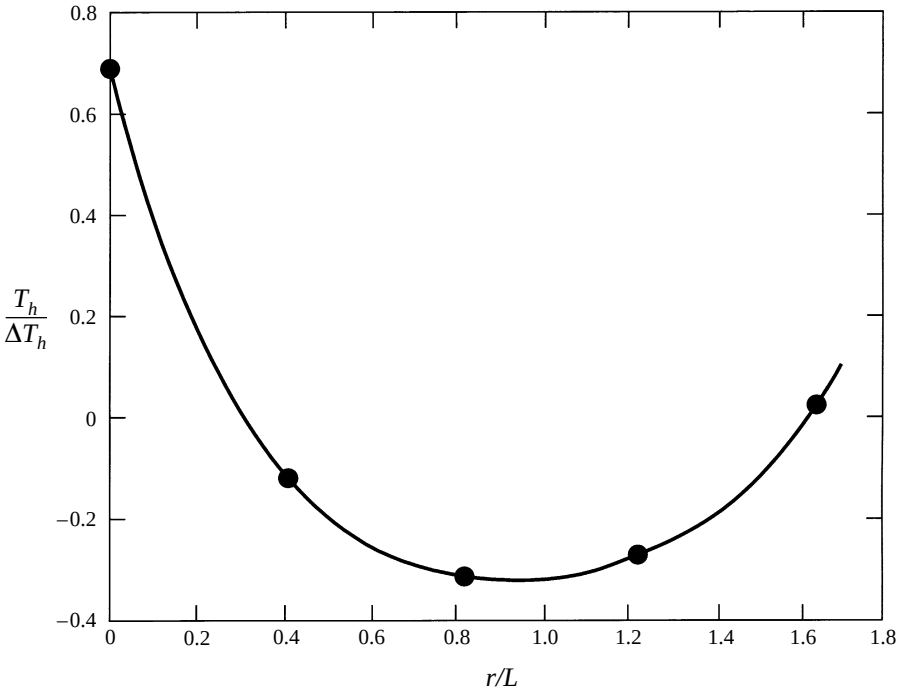

FIGURE 6. The horizontal non-dimensional distribution of temperature at the upper lid of the cylinder for experiment 12/1 of figure 3.

the meridional velocity satisfies the no-slip condition on v without the aid of an Ekman layer. The thermal wind generated in the interior bends the interior velocity profile sufficiently so that it renders v essentially zero at the top and bottom. This serves to eliminate Ekman pumping which must occur as long as σS is large compared to $E^{1/2}$.

Figure 9 shows the comparison for a case in which the stratification is much greater. This is experiment 5/16 in which $\sigma S = 168.6$. Both the experimental profiles of v in part (a) and the calculations in part (b) show, as expected, the velocity maximum to be achieved closer to the upper boundary with the core of the jet, i.e. the maximum of the velocity at about a tenth of the total depth from the surface in agreement with the estimate of the boundary layer thickness, $L/(\sigma S)^{1/2}$. Again, the comparison between theory and observation is very satisfying. Figure 9(c, d) shows the detailed comparison of the velocity profiles at $r = 2$ cm and $r = 14$ cm respectively. In the former case the theory matches the data almost exactly in the range $0.75 \leqslant z/L \leqslant 0.9$ in the region of maximum positive shear. The observation of the profile seemed to show the velocity going to zero beneath the upper boundary at about 0.5 cm from the top. At greater depth the observed dye streak seems vertical, indicating a nearly constant velocity. This seems unlikely in this high stratification limit but we have no explanation for this discrepancy. It is possible that transient effects associated with a slight alteration of the rotation rate when the thermal insulation was removed to allow data collection may be responsible. This could lead to a small uniform drift in the velocity. Figure 9(d) shows the same comparison at $r = 14$ cm. The agreement is fairly good although, again, the theory predicts a somewhat higher level for the peak of the velocity core than indicated by the measurements. Still, the overall prediction of magnitude and structure is good. Calculations of the meridional streamfunction ψ show that it has retreated to a region of about 5% of the total depth as a consequence of the stratification. Since

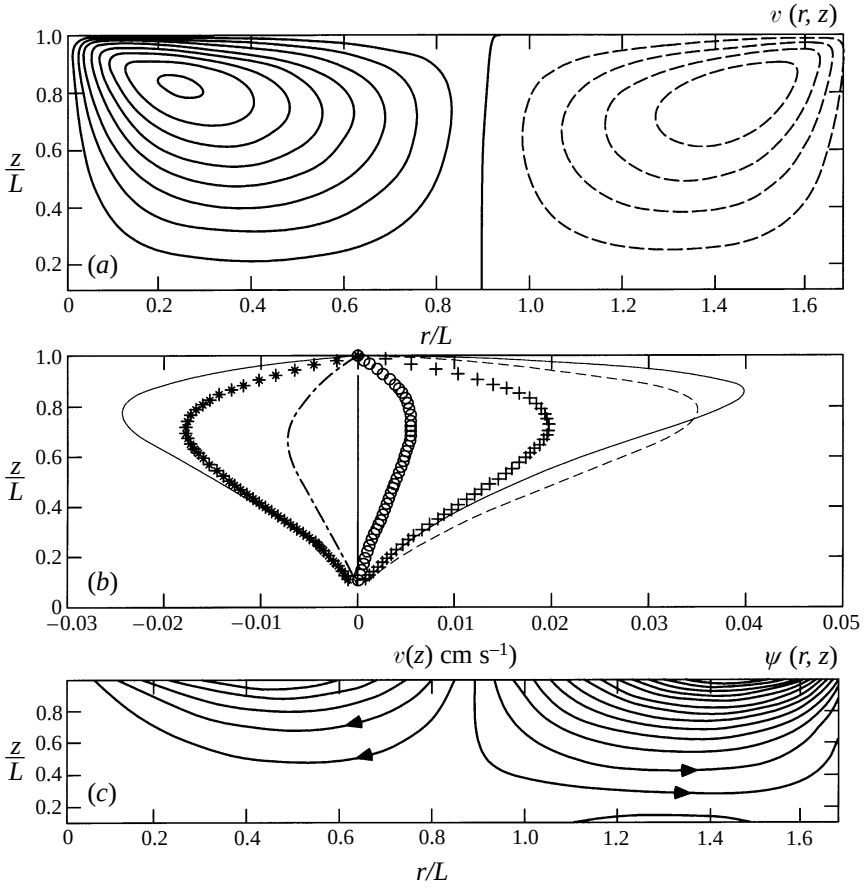

FIGURE 7. The calculated fields of motion for the 12/1 experiment. (*a*) Contours of v in the (r, z)-plane. Each contour interval is 0.005 cm s^{-1}. Negative values of v are shown by dashed contours. (*b*) Azimuthal velocity profiles at $r = 2$ (——), $r = 4$ (– –), $r = 6$ (+), $r = 8$ (○), $r = 10$ (–·–), $r = 12$ (∗), $r = 14$ (solid). (*c*) Contours of ψ.

the overall magnitude of ψ remains of $O(E)$ the radial velocity, which must be squeezed into the thermal boundary layer, has a magnitude of $E(\sigma S)^{1/2}$. This is too small to be measured. However, for large stratification its effect can be indirectly observed. We noted that the dye coming off the electrodes for this case did not remain in vertical sheets as was the case for experiments at lower stratification. Instead, the sheets seemed to twist out of the vertical plane near the upper surface and we speculate that this may be a reflection of the radial motion.

Figure 10 shows a comparison for a relatively weak stratification case (1/25) in which $\sigma S = 0.0834$ (still over 10 times greater than $E^{1/2}$). Figure 10(*a*) shows the experimental profiles, (*b*) shows the contours of v, (*c*) shows the calculated contours and (*d*) shows the meridional streamfunction. At this low value of S the velocity peak is close to mid-depth in the data. There is now a considerable quantitative discrepancy between the theory and the data. Indeed the data show the velocity greater at $r = 4$ cm than at $r = 2$ cm although the theory shows the reverse. Figure 10(*e*, *f*) shows the detailed comparison of the theory and data at $r = 2$ cm and $r = 14$ cm. Especially for the latter profile, the peak is too high in the theory as compared with the observation and the magnitude is overestimated in the theory by nearly 40 %. The disagreement is

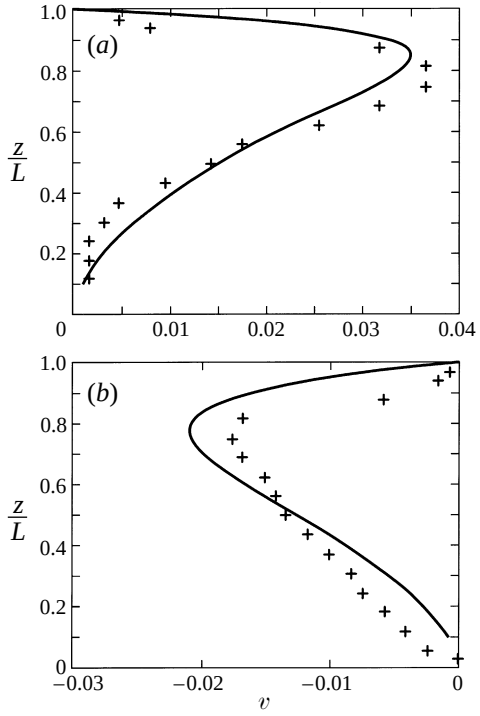

FIGURE 8. A direct comparison of theory and experiment for two profiles for experiment 12/1 for which the stratification is moderate. The experimental data are indicated by + symbols. (*a*) $r = 2$ cm, (*b*) $r = 14$ cm.

especially perplexing in this case because the Rossby number is so small. However ϵ/S is about 0.57 and so the ignored nonlinear advection in the density equation may be significant in this case.

As one anonymous reviewer has pointed out, the calculations indicate that at a radius of about 14 cm from the centre the meridional circulation is downward and is close to its maximum value. It is quite possible that the associated downward advection of the dye could contribute to the apparent discrepancy between the predicted depth of the azimuthal velocity maximum and the peak observed in the dye trace. However, this would also depend on the time between dye injection and the velocity measurement and it is difficult to quantify the effect.

The above figures show details of three typical examples of both good and fair agreement of theory and experiment. To show the results of all experiments in a compact form, values of the maxima of the azimuthal velocity for all runs and at all radii were determined from data sets like those which generated figures 3 and 9(*a*). They are compared with the maxima of predicted velocity (read from the theoretical curves such as shown in figure 7*b*) in figure 11. The correspondence between the observation and prediction is quite close in most cases. The regression coefficient to a straight line (with a slope of 1.1) is 0.93. The datum with $r = 4$ cm and prediction of 0.1 had the poorest agreement with the regression line. This run had the slowest rotation and the velocity was so great that the dye was difficult to detect and we suspect the reading of the dye edge was in error. Some of the other data with measurements of velocity less than the theory may have suffered from indistinct dye as well. The second-poorest agreement was for data with $r = 6$ cm. It seems that the core of the jet

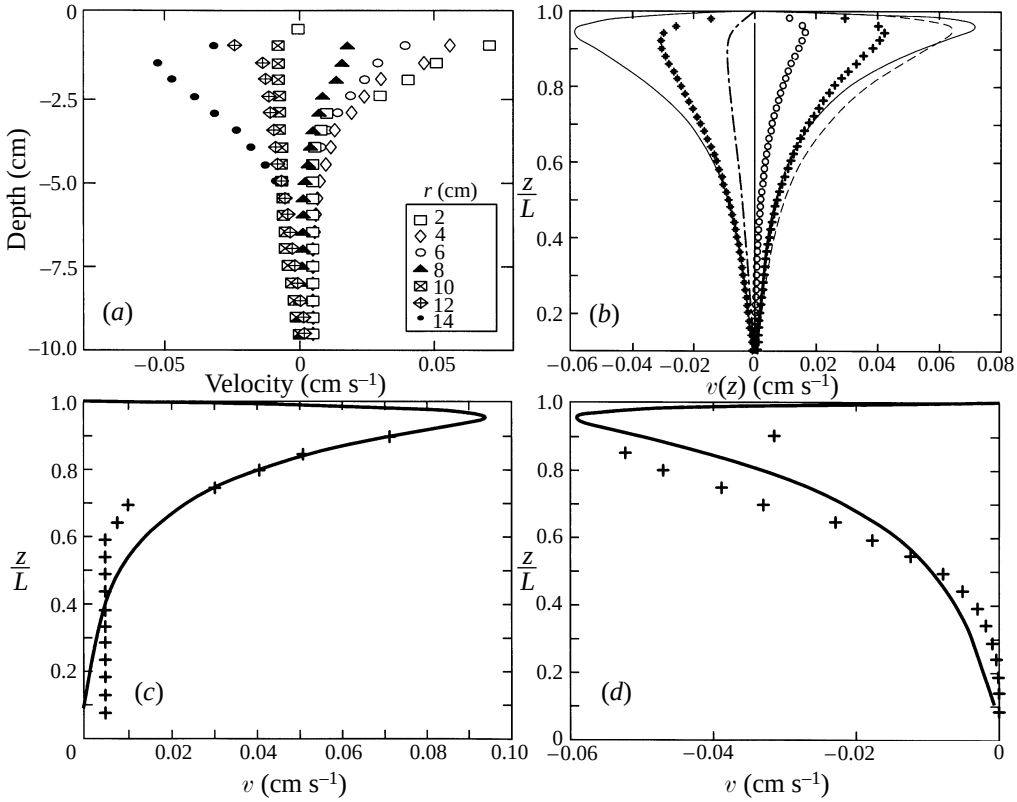

FIGURE 9. A comparison of theory and experiment for experiment 5/16 in which the stratification is large. (*a*) Experimental velocity profiles. (*b*) Calculated profiles keyed as in figure 7. (*c*) A direct comparison of theory and experiment for the profile of v at $r = 2$ cm, and (*d*) at 14 cm. The experimental data are shown with $+$.

maximum extended to that radius, somewhat beyond what the theory predicted. A thermistor reading producing a systematic error for the lid temperature is suspected as a source of error in this case.

Of course, there are other sources of error as well. We have already mentioned the warping of the lid. The presence of the electrode rods themselves will produce some heating internally as well as drag on the fluid. The vertical variation of temperature is large enough that variations of some of the fluid properties such as the Prandtl number and coefficient of thermal expansion are not completely negligible. For some of the extremely slow flows the dye streaks exhibit some signs of descent which we attribute to double-diffusive effects. We believe these latter effects are relatively small and that the discrepancies of the theory and the experiment, where they occur, are most likely due to inadequacies of the theory. Of these, the neglect of the nonlinear advection of temperature is probably the most significant. In addition, for very large σS, the thickness of the upper thermal boundary layer begins to approach the Ekman layer scale and the interaction of the two needs to be considered in more detail.

Still, the theory and experiments agree to within a few tens of percent accuracy over almost four orders of magnitude of the stratification parameter and the relative success of the linear theory in explaining the experimental results is impressive.

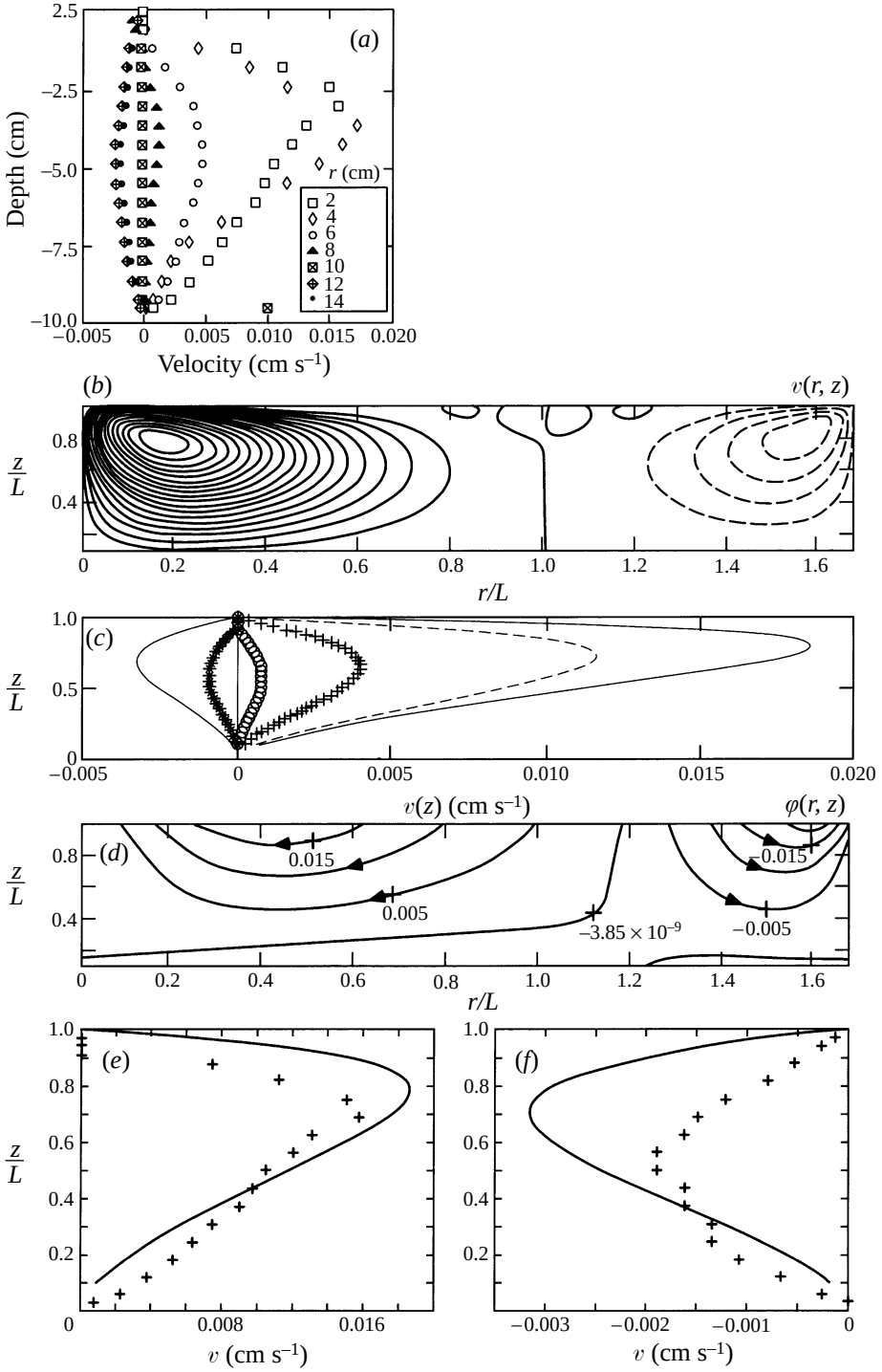

FIGURE 10. Comparison of theory and experiment for experiment 1/25 in which the stratification is weak. (*a*) Experimental velocity profiles. (*b*) Contours of velocity. (*c*) Azimuthal velocity profiles as in figure 7. (*d*) Meridional velocity streamlines. (*e*, *f*) Comparison between theory and observation for velocity profiles at 2 and 14 cm radius.

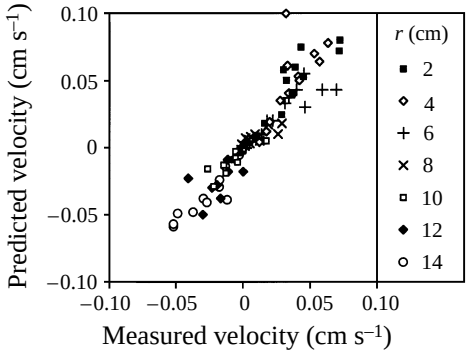

FIGURE 11. Comparison of predicted and measured values of the velocity maxima at fixed radius for all experiments listed in table 1. The radius of each measurement is shown by the symbol.

5. Discussion and conclusions

A rotating cylinder containing stratified fluid is driven by establishing at the upper surface a radially varying distribution of temperature. Linear theory has been shown to predict well the basic features of the response of the fluid to the forcing and in some cases the agreement is quantitatively excellent. One of the principal predictions of the theory is the suppression by the stable stratification of the Ekman layers as order-one elements of the dynamics. The nearly inviscid interior velocity adjusts its profile to match the no-slip boundary conditions so that the Ekman layer strength is smaller than would be anticipated by the overall mangitude of the interior velocity. The experimental results amply confirm this theoretical prediction. The interior equation of motion in the limit $\sigma S \gg E^{1/2}$ then governs the dynamics. Were the Prandtl number equal to one this would be a conduction equation for the geostrophic potential vorticity. In the case when $\sigma \neq 1$ the structure of the governing equation still emphasizes the important role that diffusion plays in determining the velocity structure. In the heated cylinder case, the direct effect of the heating and the Coriolis torque induced by the meridional motion is limited to a region whose depth shrinks to the upper surface as the stratification increases. Beneath this region the fluid is dragged along by viscous stresses from the upper flow region and the azimuthal flow in this region smoothly decreases from its maximum value in the upper thermal boundary layer to the null value on the lower surface. Because of the thermal wind relation the vertical shear in this region below the thermal boundary layer implies the existence of temperature perturbations. These, however, result from the geostrophic tilting of the otherwise flat temperature surfaces in the basic state rather than a penetration of the surface thermal forcing. We believe this basic mechanism is of potential importance in oceanic stratified flows and will serve to partially decouple the interior flow from bottom viscous effects that would normally be provided by Ekman layers.

There are several experiments similar to the ones we have already carried out that would be interesting to examine, especially in the context of comparison of theory and experiment. It would be of interest to continue to increase the lateral thermal forcing even further to enter a more radical nonlinear regime. In addition it would be of great interest to combine thermal forcing with mechanical forcing. The simplest way to include mechanical forcing would be by differential rotation of the upper lid of the container. The interplay between the two forcing mechanisms, which are purely additive in linear theory, would be interesting to examine experimentally, especially in a nonlinear regime.

It would also be of interest to return, in a more controlled manner, to driving the fluid by differentially heating the sidewalls while maintaining the overall vertical stratification. This would restore the important role of the sidewall boundary layers in the physics of the problem and would, no doubt, emphasize nonlinear effects in the neighbourhood of the boundary layers. This would especially be true for non-axially symmetric heating.

For the moment we wish only to re-emphasize that at least in this well-controlled physical environment, linear analytic theory has been remarkably successful in explaining the experimental observations of flow being independent of Ekman dynamics. Experiments at much smaller values of σS, in which there is a metamorphosis of the physical nature of the circulation from being controlled by Ekman suction, have yet to be realized.

The research of J.P. is supported in part by a grant from the National Science Foundation (OCE-9301845), J.A.W. is supported by the office of Naval Research under grant N00014-89-J1037. G.V. was supported by the Summer Student Fellowship Program of the Woods Hole Oceanographic Institution. Our sincere thanks to John Salzig who constructed the apparatus and data acquisition system, and who photographed the velocity profiles. This is Woods Hole Oceanographic Institution Contribution #9378.

REFERENCES

Barcilon, V. & Pedlosky, J. 1967*a* Linear theory of rotating stratified fluid motions. *J. Fluid Mech.* **29**, 1–16.

Barcilon, V. & Pedlosky, J. 1967*b* Unified linear theory of homogeneous and stratified rotating fluids. *J. Fluid Mech.* **29**, 609–621.

Barcilon, V. & Pedlosky, J. 1967*c* On the steady motions produced by a stable stratification in a rapidly rotating fluid. *J. Fluid Mech.* **29**, 673–690.

Bulgakov, S. N. 1987 Investigation of the haline factors in the Black Sea circulation and water structure formation. PhD thesis. Marine Hydrophysical Institute, Sevastopol, USSR.

Bulgakov, S. N., Korotaev, G. K. & Whitehead, J. A. 1996*a* The role of buoyancy fluxes in the formation of a large-scale circulation and stratification of sea water. Part 1: Theory. *Izv. Akad. Nauk SSSR Fiz. Atmos. Okeana* **32** (4), 548–556.

Bulgakov, S. N., Korotaev, G. K. & Whitehead, J. A. 1996*b* The role of buoyancy fluxes in the formation of a large-scale circulation and stratification of sea water. Part 2: Laboratory experiments. *Izv. Akad. Nauk SSSR Fiz. Atmos. Okeana* **32** (4), 557–564.

Bulgakov, S. N., Korotaev, G. K. & Whitehead, J. A. 1997 A linear model of buoyancy driven circulation in the Black Sea. *Deep-Sea Res.* (in press).

Greenspan, H. P. 1968 *The Theory of Rotating Fluids*. Cambridge University Press.

McIntyre, M. E. 1970 Diffusive destabilization of the baroclinic circular vortex. *Geophys. Fluid Dyn.* **1**, 1–57.

Pedlosky, J. 1987 *Geophysical Fluid Dynamics*. Springer.

Veronis, G. 1967 Analogous behavior of rotating and stratified fluids. *Tellus* **19**, 620–634.